

## RESEARCH ON HYDRODYNAMIC CHARACTERISTICS OF A 200 m × 175 m ANCHORED-OFFSHORE PHOTOVOLTAIC UNDER WIND-WAVE-CURRENT LOADS

Jian CHEN<sup>1</sup>, Lv REN<sup>2</sup>, Xin JIN<sup>3</sup>, Maofeng GONG<sup>4</sup>, Jie LIU<sup>5\*</sup>, Mingming LIU<sup>6</sup>

<sup>1</sup> PowerChina Hebei Electric Power Design and Research Institute Co., Ltd, Shijiazhuang 050031, China

<sup>2</sup> China Renewable Energy Engineering Institute, Beijing 100120, China

<sup>3</sup> College of Electronic Engineering, Chengdu University of Information Technology, Chengdu 610225, China

<sup>4</sup> School of Automation, Chengdu University of Information Technology, Chengdu 610225, China

<sup>5</sup> School of Mechanical Engineering, Sichuan University of Science and Engineering, Yibin 644000, China

<sup>6</sup> School of Architecture and Engineering, Liaocheng University, Liaocheng 252000, China

\*corresponding author, [pzhjeliu@126.com](mailto:pzhjeliu@126.com)

This paper presents a numerical simulation of an anchored-offshore PV under loads, using SESAM & OrcaFlex for dynamic analysis of the coupled system. It obtains forces, characteristics, and tension, and calculates the PV structure first through SESAM, then substitutes the parameters into OrcaFlex to yield the coupling model. Various conditions are considered to estimate the dynamic characteristics and obtain the operating conditions.

**Keywords:** hydrodynamic characteristics; response amplitude operator; SESAM; OrcaFlex; anchored offshore photovoltaic.



Articles in JTAM are published under Creative Commons Attribution 4.0 International. Unported License <https://creativecommons.org/licenses/by/4.0/deed.en>. By submitting an article for publication, the authors consent to the grant of the said license.

### 1. Introduction

With the increasing energy demand, the depletion of fossil energy and greenhouse gas emissions, countries are vigorously promoting the use of renewable energy. Solar energy has become one of the most applicable energy sources (Sahu *et al.*, 2016). In the past decade, the solar photovoltaic (PV) industry has experienced rapid growth and expansion of terrestrial PV due to the need to take up a large amount of land resources and therefore being limited, the floating photovoltaic (FPV) came into being. FPV uses a wide sea surface to install the PV system, with many advantages such as small water area coverage and high power generation efficiency (Vo *et al.*, 2021). According to statistics, less than 1% of the covered area can meet 25% of the world's electricity demand (Tina *et al.*, 2018). Moreover, it can integrate complementary wind, wave and tidal energy, which has huge potential for development.

PV power stations commonly adopt the underwater anchoring or shoreline anchoring, including gravity anchors, screw anchors, and pull anchors (Wu *et al.*, 2022), and the mooring system generally employs wire ropes to moor PV arrays to the anchorage points. For reasons of installation convenience, most of the completed FPV projects at home and abroad have adopted the pontoon mounting scheme (Trapani & Redón Santafé, 2015).

Lin and Liu (2019) proposed a new concept of converting a decommissioned floating liquefied natural gas system (FPSO) into an FPV platform. A PV system was designed to power the offshore platform using a frequency domain hydrodynamic analysis of the FPSO to evaluate the effect of tilt angle on energy output. Yan *et al.* (2023) proposed a new modular offshore FPV with numerical simulation and hydrodynamic coupling analysis of a multi-body FPV system. Trapani and Millar (2016) used a computational fluid dynamics (CFD) method to study the kinematic response and mooring tension of a flexible thin film PV system under the action of

regular waves. [Ikhennicheu \*et al.\* \(2022\)](#) investigated the kinematic performance of small amplitude waves (amplitude <1 m) on a 3 × 3 array FPV. [Sree \*et al.\* \(2022\)](#) proposed a methodology combining the numerical simulation and experimental validation for evaluating the kinematic and structural response of modular FPVs under wave excitations. [Xu and Wellens \(2022\)](#) analysed the nonlinear interaction of waves with an offshore FPV system.

FPV systems are growing at an astonishing rate of 133% per year over the past decade, and the total installed capacity of FPV systems globally exceeded 2.0 GW mark by the end of 2019, and reached 2.6 GW by the end of August 2020 ([Kumar \*et al.\*, 2021](#)). However, the current research is based on the hydrodynamic characteristics of monolithic structures and is dominated by lake and inland river FPV designs, and lacks the analysis of the impact on the marine environment, such as meteorological, hydrodynamic, photothermal, and submarine conditions. There is also no systematic research on the survival and operational performance of FPV power plants at sea conditions (wind, wave and current). In addition, at this stage, FPV power plants use the method of splicing PV modules, and the system's resistance to wind, wave and current performance has not been explored in depth.

In this study, the 200.0 m × 175.0 m offshore FPV system is designed. The calculations refer to the natural conditions of Zhoushan sea area in Zhejiang Province, China, including the local wind, wave and current parameters, and the amplitude response of the overall PV structure under multi-source loading and mooring forces are investigated, and reasonable mooring parameters are determined according to API RP 2SK, and the relevant results can be used for the application of the offshore PV. The results can provide a reference for the application of the offshore PV system.

## 2. Numerical methodology

Firstly, the PV model is established through SESAM/GeniE, and SESAM/HydroD is to obtain the hydrodynamic parameters of the PV structure (potential flow damping, additional mass, RAO, first-order wave force, and second-order average slow-drift force), and finally, the hydrodynamic parameters are substituted into OrcaFlex and thus yields a coupled floating body-mooring model. The coupled model is used to study the dynamic responses of the positive PV sheet, which would provide a reference for the overall development of the marine PV.

In the coupling calculation of the PV and mooring system, the interaction between the floating body and the slender body structure should be considered in each step of the iterative analysis, and the coupling influence of the floating body and the slender body structure is fully considered in Orcaflex, and the expression of the spatial discrete dynamic equilibrium control equation for the time-domain coupling analysis is as follows:

$$\mathbf{F}^I(\mathbf{r}, \ddot{\mathbf{r}}, t) + \mathbf{F}^D(\mathbf{r}, \dot{\mathbf{r}}, t) + \mathbf{F}^S(\mathbf{r}, t) = \mathbf{F}^E(\mathbf{r}, \dot{\mathbf{r}}, t), \quad (2.1)$$

where  $\mathbf{F}^I$ ,  $\mathbf{F}^D$ , and  $\mathbf{F}^S$  are the inertia force vector, damping force vector, and interaction force vector, respectively,  $\mathbf{F}^E$  is the external force vector,  $\mathbf{r}$ ,  $\dot{\mathbf{r}}$ , and  $\ddot{\mathbf{r}}$  are the displacement vector, velocity vector, and acceleration vector of the floating body structure, respectively.

$\mathbf{F}^I$  is expressed as follows:

$$\mathbf{F}^I(\mathbf{r}, \ddot{\mathbf{r}}, t) = \mathbf{M}(\mathbf{r})\ddot{\mathbf{r}}, \quad (2.2)$$

where  $\mathbf{M}$  is the mass matrix, including structural mass, fluid mass in the pipe and additional mass.

$\mathbf{F}^D$  is formulated as

$$\mathbf{F}^D(\mathbf{r}, \dot{\mathbf{r}}, t) = \mathbf{C}(\mathbf{r})\dot{\mathbf{r}}, \quad (2.3)$$

where  $\mathbf{C}(\mathbf{r})$  is the damping matrix of the system, including the structural and hydrodynamic damping.

$\mathbf{F}^S$  is calculated based on the instantaneous stress results of the unit, and  $\mathbf{F}^E$  is mainly derived from the structural gravity, buoyancy, forced displacement, environmental forces, and other specific loads.

Formulas of the wind force and moment for PV structures are, respectively, as follows:

$$F_{XW} = \frac{1}{2}C_{XW}\rho_W V_W^2 A_T, \quad (2.4)$$

$$F_{YW} = \frac{1}{2}C_{YW}\rho_W V_W^2 A_L, \quad (2.5)$$

$$M_{XYW} = \frac{1}{2}C_{XYW}\rho_W V_W^2 A_L L_{BP}, \quad (2.6)$$

where  $F_{XW}$ ,  $F_{YW}$ , and  $M_{XYW}$  are the longitudinal wind force, transverse wind force and bow-wake wind moment, respectively,  $C_{XW}$ ,  $C_{YW}$ , and  $C_{XYW}$  are, respectively, the longitudinal wind force coefficient, the transverse wind force coefficient and the bow-wake wind moment coefficient, where the wind force coefficient is obtained by referring to the plots in the [Oil Companies International Marine Forum \[OCIMF\] \(1994\)](#) data,  $\rho_W$  is the air density;  $V_W$  is the wind speed at 10 metres above the sea level,  $A_T$  is the forward wind area,  $A_L$  is the lateral wind area,  $L_{BP}$  is the length between plumb lines.

The flow rate is modelled using a power function (power law function), as follows:

$$S = S_b + [(S_f - S_b) \times (Z - Z_b)/(Z_f - Z_b)]^{1/7}, \quad (2.7)$$

where  $S_b$  and  $S_f$  correspond to the bottom flow velocity and surface flow velocity,  $Z_b$  is the height of the still water surface,  $Z_f$  is the depth of the seabed.

The longitudinal flow force  $F_{XC}$ , the transverse flow force  $F_{YC}$  and the bow-wake flow moment  $M_{XYC}$  for PV structures are, respectively, estimated through the formulas:

$$F_{XC} = \frac{1}{2}C_{XC}\rho_C V_C^2 T B, \quad (2.8)$$

$$F_{YC} = \frac{1}{2}C_{YC}\rho_C V_C^2 T L_{BP}, \quad (2.9)$$

$$M_{XYC} = \frac{1}{2}C_{XYC}\rho_C V_C^2 T L_{BP}^2, \quad (2.10)$$

where  $C_{XC}$ ,  $C_{YC}$ , and  $C_{XYC}$  are the longitudinal flow coefficient, transverse flow coefficient, and bow hook moment coefficient, respectively, and the flow coefficients are obtained by referring to the plots in the [OCIMF \(1994\)](#) data;  $\rho_C$  is the density of seawater, and  $V_C$  is the flow velocity;  $T$  is the draught;  $B$  is the width.

### 3. Computational parameters

#### 3.1. Study region and designed cases

The 200.0 m × 175.0 m PV monolithic structure is considered, with the operating environment being designed with reference to the sea conditions in Zhoushan, Zhejiang Province, China. The water depth of  $h = 15.0$  m is applied. Three different wave conditions are considered, which are generated by JONSWAP spectra with effective wave heights of 1.5 m, 2.0 m, and 2.5 m, corresponding to wave periods of 5.0 s, 6.0 s, and 7.0 s, as well as three wind speed conditions (10.0 m/s, 20.0 m/s, and 30.0 m/s) and two current conditions (0.5 m/s and 1.0 m/s). A total of 18 operational conditions are simulated, as shown in [Table 1](#).

Table 1. Operational cases in wind-wave-current sea conditions.

No.	Significant wave height [m]	Peak frequency [s]	Flow velocity [m/s]	Wind velocity [m/s]
LC1~LC3	1.5	5.0	0.5	10.0/20.0/30.0
LC4~LC6	1.5	5.0	1.0	10.0/20.0/30.0
LC7~LC9	2.0	6.0	0.5	10.0/20.0/30.0
LC10~LC12	2.0	6.0	1.0	10.0/20.0/30.0
LC13~LC15	2.5	7.0	0.5	10.0/20.0/30.0
LC16~LC18	2.5	7.0	1.0	10.0/20.0/30.0

### 3.2. Model geometric parameters and modelling

The PV system consists of  $100 \times 100$  PV basic blocks, which are rigidly connected without considering the influence of mutual movement of structures. The computational model simplifies the PV overall and individual structural forms and ignores the PV detailed structures, thus reducing the mesh quantity, and the PV wet-surface, and the mass model is built by SESAM/GeniE, and the PV model and the individual sheet mesh model are shown in Fig. 1.

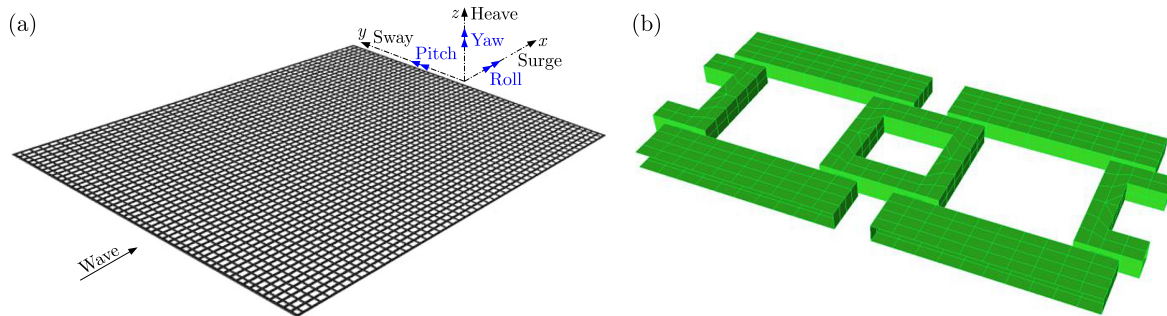


Fig. 1. Model of offshore PV structure: (a) panel model; (b) individual photovoltaic grid models.

Table 2. Overall structure of anchored offshore PV system.

Length [m]	Width [m]	Draft [m]	Discharge [ton]	Centre of gravity height from baseline [m]	Wind area in longitudinal [m <sup>2</sup> ]	Wind area in transverse [m <sup>2</sup> ]	Flow area in longitudinal [m <sup>2</sup> ]	Flow area in transverse [m <sup>2</sup> ]
200	175	0.2	463	0.2	75.4	21	40	35

The simulation is divided into the static and dynamic analyses. The static analysis considers the average loads of wind, current and drift forces acting on the PV and the mooring cable as well as external loads, and the calculated average offset position of the PV system and the mooring cable tension are used as the starting position for the subsequent dynamic analysis. The dynamic analysis takes into account the dynamic effects of the PV structure, the mooring cable and the external loads to obtain the displacement of the structure and the mooring cable tension.

### 3.3. Mooring scheme

The PV structure is fixed by mooring positioning, and the seabed is anchored by concrete blocks (the gravity of the concrete blocks is much greater than the tension of the anchor chains). The mooring chain is distributed along the perimeter of the PV, and the anchor chain is set at the chain exit to the anchorage point, with a diameter of 0.04 m, a length of 32.0 m, and a spacing of 20.0 m, for a total of 40 anchor chains. The parameters of the mooring chain and the deployment are, respectively, shown in Table 3 and Fig. 2.

Table 3. Properties of mooring chains.

Cable length [m]	Diameter [m]	Air quality [kg/m]	Water quality [kg/m]	Axial stiffness [N]	Breaking force [kN]	Drag coefficients	Added mass coefficients
32	0.04	31.8	27.7	1.37e8	1280	(2.6, 2.6, 1.4)	(1.0, 1.0, 0.5)

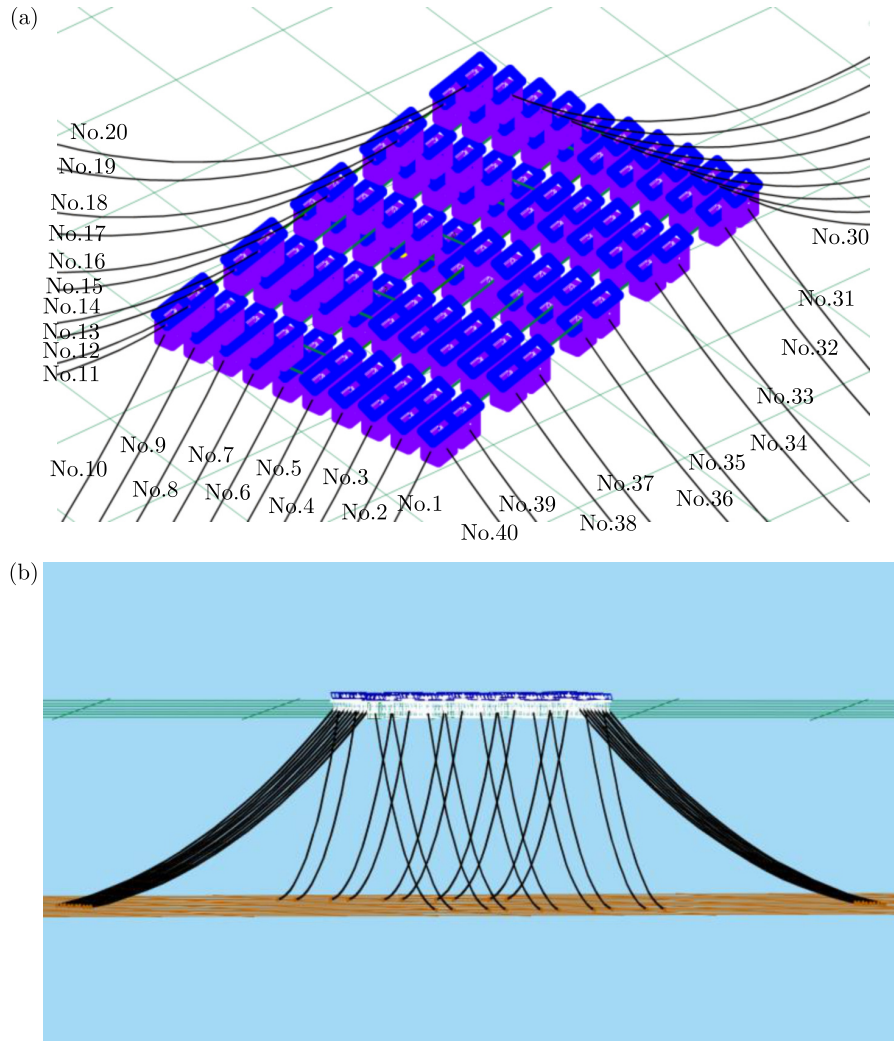


Fig. 2. Schematic map of the mooring chain: (a) over view; (b) front view.

### 3.4. Safety specification

The main constraints of the coupled dynamic analysis of photovoltaics and mooring chain are the mooring cable tension, the anchor grip, and the float motion response. Since the large long-period slow-drift motion of the float has less impact on the upper PV structure, and the present PV anchoring method is simplified as fixed, the mooring cable tension is the main concern in the calculation.

Minimum Safety Factor for Mooring Cable Referring to API RP 2SK Specification (OCIMF, 1994) and China Classification Society [CCS] (2019) specification require that the mooring cable tension must satisfy a certain safety factor. The ratio of the breaking load of the mooring cable to the maximum design tension represents the safety factor (SF), i.e.,  $SF = \text{breaking load} / \text{maximum design tension}$ . The results listed in the paper are that after taking into account the dynamic amplification factor, which is a dynamic calculation, the minimum safety factor for normal operating conditions is set as 1.67.

## 4. Results and discussion

### 4.1. Frequency domain characteristics

SESAM is used to carry out the frequency domain characteristics of the PV structure to obtain the hydrodynamic parameters. Regular waves are chosen for the frequency domain calculation, the wave frequency ranges from 0.2 rad/s to 1.8 rad/s with an interval of 0.05 rad/s, and the wave incidence direction ranges from  $0^\circ$  to  $180^\circ$  with an interval of  $15^\circ$ .

The six-degree-of-freedom (surge, sway, heave, roll, pitch, and yaw) response amplitude operators (RAOs) of the PV structure under different wave incidence conditions are illustrated in Fig. 3. From the figure, it can be seen that the RAOs of both surge and sway decrease with the increase of the wave frequency. We can also find that both RAOs are almost identical, which is mainly due to the fact that the PV structure is close to the square; the maximum surge

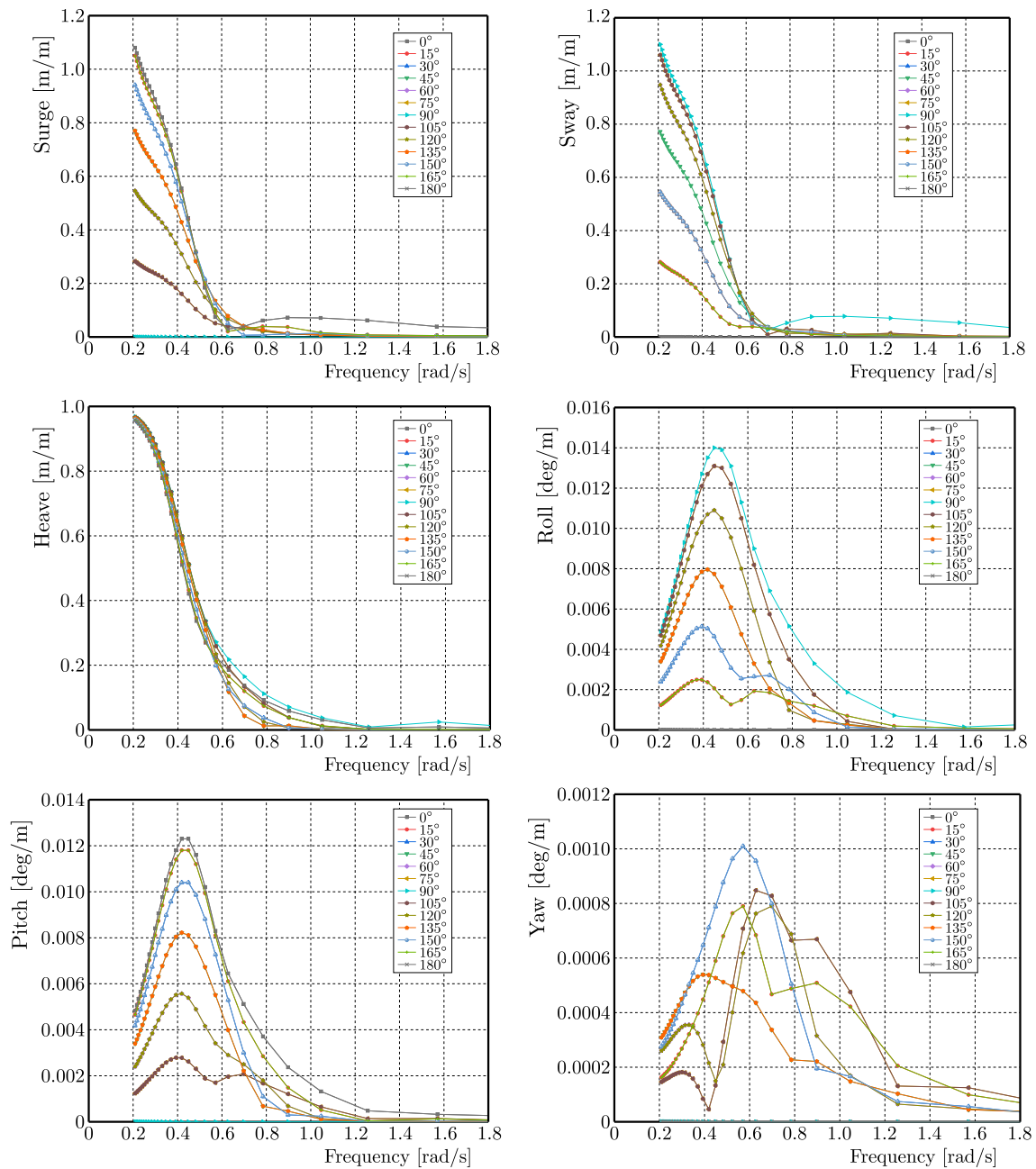


Fig. 3. Variations of response amplitude operator (RAO) with wave frequency under various wave direction angles.

RAO for different wave directions occurs at  $0^\circ$  or  $180^\circ$  wave direction angle, while the maximum sway RAO for different wave directions occurs at  $90^\circ$  wave direction angle. Besides, the surge is sensitive to the low-frequency wave below 0.6 rad/s, and the facing and following waves have the greatest influence on the surge, while the transverse wave has almost no influence. Similar to that of the surge, the sway is also sensitive to the wave frequency of less than 0.6 rad/s. But, contrary to that of the surge, the transverse wave influences on the sway greatly, while the influence of the wave facing and following is weak. In heave motion, the amplitude of each wave angle decreases with the increase of wave frequency, the heave RAOs of all wave directions are almost the same, and no resonance appears. Therefore, the PV structure is not sensitive to the wave resonance frequency.

For both roll and pitch, the RAOs at each wave direction angle show a tendency of increasing and then decreasing with the increasing wave frequency. The sensitive frequency of roll and pitch RAOs corresponds to 0.524 rad/s, where the maximum roll RAO appears at  $90^\circ$  wave direction angle, while the maximum pitch RAO occurs at  $0^\circ$  and  $180^\circ$  wave direction angles. The maximum yaw RAO occurs at  $150^\circ$  wave direction angle, which corresponds to a wave frequency of 0.58 rad/s.

The above discussions reveal that the planar responses are much fiercer than the rotational motions, thus the planar motions of the PV structure are the main controlling factor for the tension of the mooring chain.

#### 4.2. Time domain characteristics

The coupled dynamic analysis of moored floating body is based on Orcaflex, the pre-tension of the mooring chain is about 10 tons in the simulation, in which the JONSWAP spectrum is selected to generate random waves. The frequency domain hydrodynamic parameters of the PV structure are substituted into Orcaflex, and the integrated effects of the environmental forces of the wind, wave, and current are considered to carry out the time-domain dynamic analysis under anchored conditions, to obtain the time series of the force acting on the anchored cable. Finally, the maximum tension of the anchored cable and the operational response of the anchored-offshore PV system are obtained according to the 3.0 hours' regression period.

In the calculation, the most dangerous working condition is considered to be the coincident incidence of wind, wave and current, and then the coupled dynamics of the floating body-anchor chain is solved. Reference is made to the API RP 2SK Specification (OCIMF, 1994), and five different wave seeds are calculated, respectively, in the simulation of irregular waves, and the anchored chain tension is chosen as the average value of five runs to reduce the randomness of irregular waves.

For demonstration, the dynamic response of the PV system at a certain time instant is demonstrated in Fig. 4. From this figure, the anchored chain in the environmental incidence

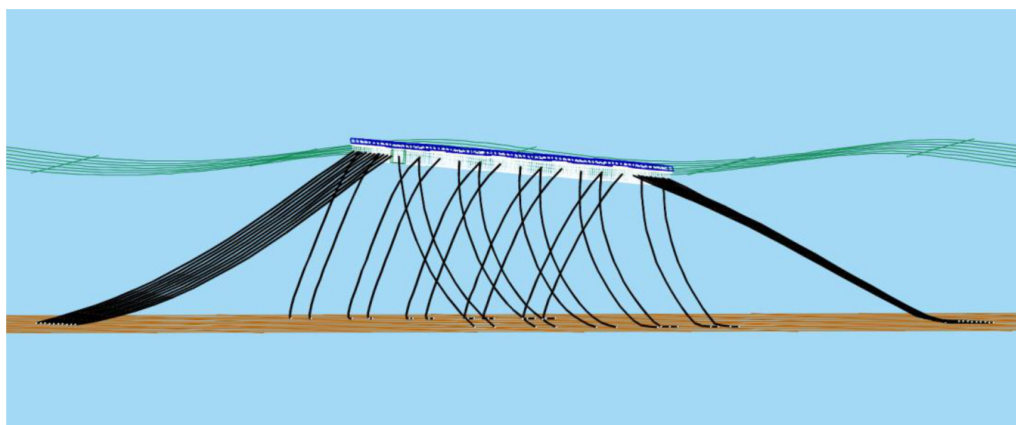


Fig. 4. Schematic map of the dynamic response of the PV system at a certain time instant.

direction is in a tense state, while the anchored chain in the propagation direction is in a relaxed state. Due to the overall rigidity of the PV system, the draft of the PV structure in the environmental incidence direction increases, thus increasing the force on the anchored cable, so the anchored chain is in a tense shape.

Figure 5 shows the time series of the wind force, current force, first order wave force and the second order slow drift force on the PV structure of Case 12. It can be seen from this figure that the PV structure is subjected to the largest first-order wave force with a maximum of about 15000 kN, the wind force is about 5.18 kN, and the second-order wave force of the slow drift approaches 540 kN. The current force is the minimal, being 0.288 kN. Therefore, by comparisons, it can be concluded that the main controlling factor of the system is the first-order wave force, and therefore the design should be focused on considering the effect of its impacts on the mooring equipment.

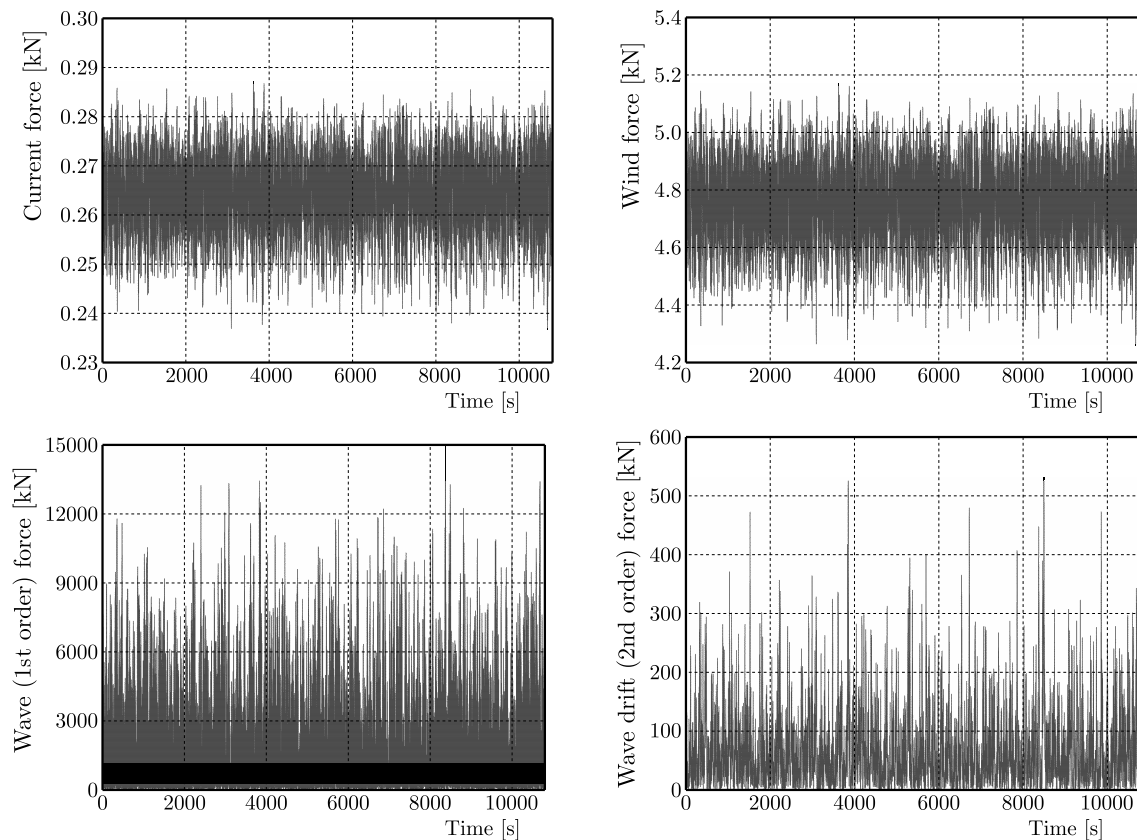


Fig. 5. Time series of current, wind and wave loads on the PV structure.

Table 4 gives the effective tensions of the maximum tension of the anchor chain under five wave seeds with the wave heights of 1.5 m, 2.0 m, and 2.5 m. From this table, it can be seen that the working conditions of LC1 to LC6 with the wave height of 1.5 m, the maximum tension of the anchor cable is 324.0 kN, and the corresponding safety factor is 4.85, which can meet the

Table 4. Maximum tension of cable chains.

Working condition	Mooring chain [kN]						Safety factor
	Seed 1	Seed 2	Seed 3	Seed 4	Seed 5	Mean value	
LC6	202	324	276	233	285	264	4.85
LC12	945	1230	1002	960	923	1012	1.26
LC18	2430	2675	2560	2468	2617	2550	0.5

requirement of the safety factor 1.67; for the working conditions of LC7 to LC12 with the wave height of 2.0 m, the maximum tension of the anchor cable is 1012.0 kN, with the corresponding safety factor being 1.26, which no longer satisfies the safety factor 1.67. As for the working conditions of LC13 to LC18, the wave height being 2.5 m, the maximum anchor cable tension is 2550.0 kN, yielding the safety factor being 0.5, which also does not guarantee the specification requirements. Therefore, the anchored chain with the diameter 40.0 mm cannot meet the safety requirements of 2.0 m and 2.5 m wave height' operation conditions. To meet the operation requirement of 1.67, a cable with a diameter of at least 48.0 mm should be selected for 2.0 m wave height, and for 2.5 m wave height, a cable with a diameter of at least 76.0 mm diameter is needed.

The time series of the maximum dynamic tensions of the anchored cable for LC6, LC12, and LC 18 of the wave seed 2 are shown in Fig. 6. The figure shows that the maximum tension is at the transient stage, which exhibits one or several peaks, and the tension oscillates up and down in a certain equilibrium position, which is consistent with the large-value planar motion of the PV structure.

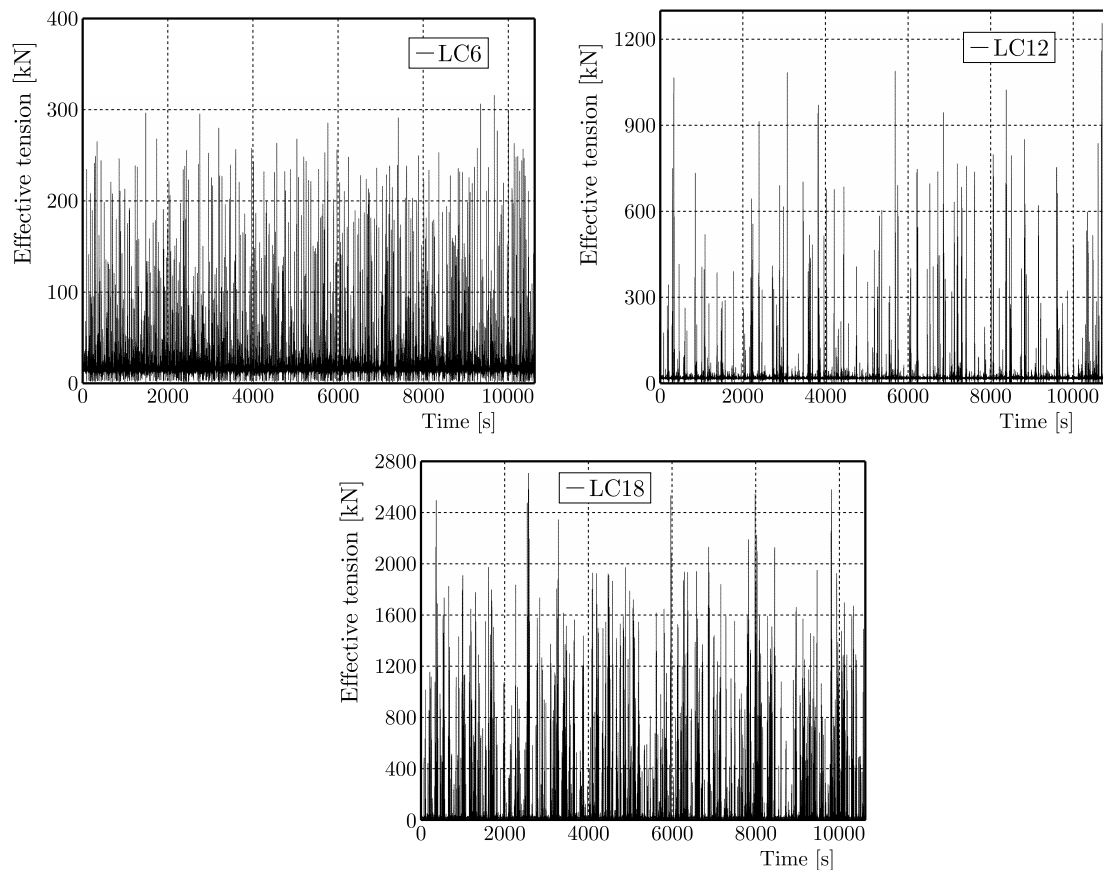


Fig. 6. Time series of anchored cable tension.

## 5. Conclusions

This study carries out the time-domain coupled dynamic characterization of a 200.0 m × 175.0 m anchored-offshore PV system based on the potential flow theory, and the dynamic response characteristics of the PV structure under the combined effects of wind, wave and current loads are obtained. And, the optimal anchored chain parameters are identified based on the API RP 2SK specification (OCIMF, 1994). The conclusions are as follows:

- 1) The designed PV structure has no significant wave resonance characteristics. Since the PV structure is close to a square, its transverse and longitudinal oscillation RAOs are

- basically the same, and the transverse and longitudinal oscillation RAO trends are also the same. Moreover, since the longitudinal and transverse areas of the PV sheet are large, their frequency domain characteristics show no obvious wave resonance characteristics.
- 2) Wave load is the main factor affecting the mooring cable tension. Due to the shallow draft and small wind area of the PV, its wind and current loads are significantly smaller than the wave loads, and the wind and current loads have less influence on the dynamic maximum tension of the mooring cable.
  - 3) This design of 40.0 mm anchor chain can meet the operational requirements of working conditions LC1~LC6, but is invalid for working conditions LC7~LC18. When the environmental load is 2.0 m wave height, 1.0 m flow velocity, 30.0 m/s wind speed operating conditions, the minimum diameter of the anchored chain should be selected as 48.0 mm; when the environmental load is 2.5 m wave height, 1.0 m flow velocity, 30.0 m/s wind speed operating conditions, the diameter of the anchored chain should be no less than 76.0 mm.

### Acknowledgments

The work was supported, in part, by the National Natural Science Foundation of China (grant no. U2342216), Key R&D program of Science & Technology Department of Sichuan Province (grant no. 2024YFHZ0173), Science Foundation of Science & Technology Department of Sichuan Province (grant no. 2023NSFSC0747), and the Ministry of Education Collaborative Education (grant no. 230806521252005, 231006521163646).

### References

1. China Classification Society [CCS]. (2019). *Classification specification for offshore mobile platforms*.
2. Ikhennicheu, M., Blanc, A., Danglade, B., & Gilloteaux, J.-C. (2022). OrcaFlex modelling of a multi-body floating solar island subjected to waves. *Energies*, 15(23), Article 9260. <https://doi.org/10.3390/en15239260>
3. Kumar, M., Niyaz, H.M., & Gupta, R. (2021). Challenges and opportunities towards the development of floating photovoltaic systems. *Solar Energy Materials and Solar Cells*, 233, Article 111408. <https://doi.org/10.1016/j.solmat.2021.111408>
4. Lin, Z. & Liu, X. (2019). Sustainable development of decommissioned FPSO as a floating solar plant – case study of the effects of tilt angle on energy efficiency. *Proceedings of the International Conference on Applied Energy*, Västerås, Sweden (4, Article 0468).
5. Oil Companies International Marine Forum [OCIMF]. (1994). *Prediction of wind and current loads on VLCCs* (2nd ed.). London, England: Witherby.
6. Sahu, A., Yadav, N., & Sudhakar, K. (2016). Floating photovoltaic power plant: A review. *Renewable and Sustainable Energy Reviews*, 66, 815–824. <https://doi.org/10.1016/j.rser.2016.08.051>
7. Sree, D.K.K., Law, A.W.K., Pang, D.S.C., Tan, S.T., Wang, C.L., Kew, J.H., Seow, W.K., & Lim, V.H. (2022). Fluid-structural analysis of modular floating solar farms under wave motion. *Solar Energy*, 233, 161–181. <https://doi.org/10.1016/j.solener.2022.01.017>
8. Tina, G.M., Cazzaniga, R., Rosa-Clot, M., Rosa-Clot, P. (2018). Geographic and technical floating photovoltaic potential. *Thermal Science*, 22(Suppl. 3), S831–S841. <https://doi.org/10.2298/TSCI170929017T>
9. Trapani, K. & Millar, D.L. (2016). Hydrodynamic overview of flexible floating thin film PV arrays. *Proceedings of the 3rd Offshore Energy and Storage Symposium*, Valletta, Malta.
10. Trapani, K. & Redón Santafé, M. (2015). A review of floating photovoltaic installations: 2007–2013. *Progress in Photovoltaics: Research and Applications*, 23(4), 524–532. <https://doi.org/10.1002/pip.2466>

11. Vo, T.T.E., Ko, H., Huh, J., & Park, N. (2021). Overview of possibilities of solar floating photovoltaic systems in the offshore industry. *Energies*, 14(21), Article 6988. <https://doi.org/10.3390/en14216988>
12. Wu, X., Xiao, W., Yang, L., & Pan, Y. (2022). Research on hydrodynamic characteristics of an offshore flexible floating photovoltaic in waves. *2022 3rd International Conference on Geology, Mapping and Remote Sensing (ICGMRS)*, Zhoushan, China, 841–845. <https://doi.org/10.1109/ICGMRS55602.2022.9849362>
13. Xu, P. & Wellens, P.R. (2022). Theoretical analysis of nonlinear fluid-structure interaction between large-scale polymer offshore floating photovoltaics and waves. *Ocean Engineering*, 249, Article 110829. <https://doi.org/10.1016/j.oceaneng.2022.110829>
14. Yan, C., Shi, W., Han, X., Li, X., & Verma A.S. (2023). Assessing the dynamic behaviour of multi-connected offshore floating photovoltaic systems under combined wave-wind loads: A comprehensive numerical analysis. *Sustainable Horizons*, 8, Article 100072. <https://doi.org/10.1016/j.horiz.2023.100072>

*Manuscript received April 30, 2024; accepted for publication January 3, 2025;  
published online March 24, 2025.*

